Jurnal Mekanikal
Disember 2002, Bil. 14, 1 - 20

RADIAL STRAIN RELAXATION IN A COLD WORKED ALUMINIUM ALLOY 2024-T351 PLATE SPECIMEN

Prithvi Raj Arora[1]
Ram Kumar Krishnasamy
Jeffrey Tan Meng Lee

Department of Aerospace Engineering
University Putra Malaysia
Serdang, Malaysia

ABSTRACT

Aluminium alloy 2024 T351 is used for carrying out cold work experiment. Altogether 16 strain gauges have been mounted in the radial direction to measure the radial strain distribution using HP data acquisition system and Visual Engineering Environment (VEE) software. The strain distribution was recorded under different conditions of cold working process. The value of elastic-plastic boundary experimentally measured matches well with the existing theories of Nadai, Chang, and Rich and Impellizeri. The experimental residual strain distribution results compares very well with the Finite Element Method (FEM) results particularly for a case of full mandrel removed condition. The recommendation is made to use the strain relaxation data for a case where the mandrel need not be removed after cold working for accessing the residual strain distribution in the specimen.

1.0 INTRODUCTION

The presence of fastener holes in a structural component is responsible for lowering its fatigue life. Under cyclic loading conditions, fatigue crack usually starts at the edge of the hole, which is the location of stress concentration, and then slowly spreads through the whole thickness of the component [1]. In order to minimize the detrimental effect of the stress concentration, it is a common practice to prestress or cold work the region of high stresses. Stress coining is one of the cold working processes and consists of pulling an oversized mandrel through the fastener hole. The process of drawing the mandrel through the fastener hole results in a radial flow of the metal. The subsequent removal of the mandrel unloads the plastically deformed metal thereby introducing residual compressive stress around the hole region. This alleviates the mean stress levels in cyclic loading, which results in increased fatigue life. This increase in fatigue life has been demonstrated for various materials by different cold working processes. It is indeed a difficult task to obtain the optimum amount of cold work leading to optimum fatigue properties. Usually, it is done through varied trials of

[1] Author to whom all the correspondence should be addressed; Tel: 603-89466404, e-mail; prithvi@eng.upm.edu.my

fatigue tests for several levels of cold work. Finally, the cold work parameters that lead to better fatigue properties are selected. This does not provide insight into the mechanics of the cold working process. Though various theories [2] have been developed to predict the elastic-plastic boundary and residual stresses, to date, no formulation exists which correlates well with the experimental results.

The purpose of this investigation is to survey the existing theoretical and experimental work related to residual strain distribution and evaluation of elastic-plastic boundary during a cold working process. A cold working experiment is conducted to determine the radial residual strain distribution at various stages of cold working and hence to formulate a model to predict the elastic-plastic boundary based on the experimental investigation using the 2024 T351 aluminium alloy. The experimental results are to be compared with the FEM and theoretical formulations.

2.0 EXPERIMENTAL SETUP

2.1 Materials and the Specimen

Aluminium alloy 2024-T351material is used in the plate form with 6.35mm thickness. The mechanical properties of the material are obtained from the standard tension test samples prepared along the rolling direction of the plate and are given in Table 1. Four holes of 5.8mm diameter were drilled in the specimen and finally they were reamed to 6.0 mm diameter. The other geometrical details of the specimens for cold working are given in Figure 1.

2.2 Strain Gauge Installation

To measure the radial strain around the hole region after cold working it is necessary to organise the location of the strain gauges. The location of the gauges have been planned (Figure 2) to accommodate more number of gauges in the radial direction. A half bridge configuration was used for strain gauge measurement for temperature compensation. The specimen surface near the vicinity of the hole was roughened by 200 grade emery paper, cleaned with carbon tetrachloride (CCl_4) and subsequently marked as per the strain gauge mounting layout shown in Figure 2. The general dimensions of the base and grid including the gauge factor, GF are given in Table 2. The Cu-Ni foil strain gauges supplied by Tokyo Sokki Kenkyujo Co. LTD, Japan were mounted using Cyanoacrylate cement (CN). The cement has a curing time of 1 min and the operating temperature range is –30 to +100°C. The distance of the gages from the edge of the hole was measured to an accuracy of 0.01 mm. Altogether sixteen strain gauges are used to get the radial strain at different radial distance from the edge of the hole. The numbers appearing on the layout (Figure 2) represent the number of strain gauges given in the first column of Table 2.

2.3 Cold Working Process

In the cold working process, a large size mandrel is inserted through the hole of relatively smaller diameter and it is shown schematically in Figure 3. The sleeve is first inserted in the hole which acts as a surface protector to the hole surface from the anticipated damage caused by mandrel insertion and then the mandrel is registered on the mouth of the hole indicating the initial engagement of the mandrel with the specimen (Figure 3a). Next, the mandrel is pushed through till the center of the maximum diameter region of the mandrel coincides with the mid thickness of the plate specimen (Figure 3b). Finally, the mandrel is pushed further disengaging it from the hole (Fig.3c) imparting the radial expansion to the specimen material around the hole region. The initial diameter of the hole was measured at two orthogonal locations and its average value was used for the calculation of cold work. The thickness of the sleeve used in our investigation is 0.2 mm. The final hole diameter under fully expanded hole condition is calculated by adding twice the sleeve thickness to the maximum mandrel diameter and is used for the calculation of cold work by the following equation:

$$\text{Cold work} = \frac{\text{Final hole diameter} - \text{Initial hole diameter}}{\text{Initial hole diameter}} = \frac{\text{Radial expansion}}{\text{Initial hole radius}} = \frac{u_a}{r} \tag{1}$$

where, u_a is the radial expansion.

2.4 Calibration Procedure

The gauge factor of strain gauges [3] is given by the following equation and its value is given by the strain gauge manufacturer.

$$GF = \frac{\partial R / R}{\partial l / l} = \frac{\text{Relative change in resistance}}{\text{Strain}} \tag{2}$$

For calibration purpose, the theoretical strain is calculated by the following equation and this equation is developed by shunting one of the arm of the Wheat stone bridge [3] by a calibration resistance R_{cal},

$$\varepsilon = \frac{1}{GF}\left[\frac{R}{R + R_{cal}}\right] \tag{3}$$

where,
GF is the gauge factor of the strain gauge, and R is the strain gauge resistance.

The voltage output from the half bridge configuration obtained experimentally by shunting one of the arm of the Wheat stone bridge should correspond to the theoretically calculated strain by equation (3) giving the calibration [3] of the Wheat stone bridge system used for strain measurement in this investigation.

2.5 Stages of cold work

Changes in voltage signal (Wheat stone bridge output) were extracted for 5 different stages (Figure 4) during the cold working process. The first stage marked as 1 in Figure 4 represents the start of the record for the input voltage signal as received from the Wheat stone bridge used for measurement of strain. The second stage represents offsetting the input voltage signal to make it zero for the recording purpose and is marked as 2 in Figure 4. The stage three represents the voltage signal corresponding to the maximum mandrel insertion position and is marked as 3 in Figure 4. The stage four represents the relaxation in voltage signal when the mandrel is still in the maximum insertion position i.e. in the middle of the plate specimen and is marked as 4 in the Figure 4. The stage five represents the voltage signal when the mandrel is fully removed from the expanded hole of the specimen and it is marked as 5 in Figure 4. The curve beyond the stage five or point 5 (Figure 4) represents the relaxation in the voltage signal and in the present case it is observed to be practically negligible. Hence the voltage signal represented by point 5 (Figure 4) is the signal corresponding to the mandrel-removed condition. These voltage signals are converted to strain signals making use of calibration technique described in Section 2.4. The calibration constants can vary to some extent as they depend on the resistance of the strain gauge used. An individual strain gauge measurement point represents a different strain gauge installation constituting an individually different Wheat stone bridge circuitry, and hence giving different calibration constants. These calibration constants for different gauge locations are given in Table 2. HP data acquisition system using Visual Engineering Environment (VEE) program has been used in this investigation for acquiring and recording the voltage signal obtained from the Wheat stone bridge circuitry. The rate of loading used in this experiment is 100N/s. The output voltage signal in Figure 4 corresponds to the output from the strain gauge number 1.

3.0 THEORIES OF RESIDUAL STRESSES AROUND A COLD WORKED HOLE

Some prominent theories for estimating the radius of the elastic-plastic boundary around the cold worked region of fastener holes are given in this section. The purpose of these theories is to get an estimate of an elastic-plastic boundary for a given value of radial expansion, u_a imparted to the hole periphery during the cold working process. Some theories are given as a function of non-dimensional radial displacement, u_a/u_{aE}, where u_{aE} is the largest radial displacement, [4] that can be

applied to the edge of the hole without causing plastic deformation and is given by the following equation,

$$u_{aE} = \frac{(1+\nu)\sigma_o a}{E\sqrt{3}} \tag{4}$$

where, σ_0 is the yield stress and a is the radius of the hole.

Once u_a becomes greater than u_{aE}, the material at the edge of the hole becomes plastically deformed out to a radius r_p – the elastic–plastic boundary. Once the hole has been expanded to the prescribed radial displacement, u_a, giving the required cold-work, upon unloading i.e. removing radial displacement, u_a gives rise to residual stresses around the hole region. Most of these theories represent this unloaded condition of the material around the cold-worked hole region.

3.1 The Nadai Theory

Nadai [5] developed a theory of plastic expansion of small tubes fitted into boiler heads. He considered the plastic deformation of both the plate and tubes. His assumptions were as follows:

1. The problem corresponds to that of a uniform pressure at inside edge of the hole in an infinite plate under a state of plane stress.
2. Initiation of plastic yielding is based on Mises-Hencky yield criterion.
3. The material response is perfectly plastic.

He developed a relationship to estimate the radius of the elastic-plastic boundary based on his earlier work

$$r_p = a / \exp\left\{\frac{3}{2}\left[\left(\frac{u_a}{u_{aE}}\right)^{1/3} - 1\right]\right\} \tag{5}$$

The simplicity of this formula makes this theory very easy to use.

3.2 The Chang Theory

Chang [1] used the elastic-plastic solution of pressurized thick walled cylinder of Hoffman and Sachs to compute the residual stress distribution to an open hole in a thick plate and then used it for an analytical prediction of fatigue crack growth of cold worked holes. The assumptions of this theory were as follows:

1. The material is perfectly plastic.
2. Plane strain condition is valid under uniform pressure at the hole edge.
3. Yielding is based on Mises-Hencky criterion.

The relation between the u_a and r_p is

$$u_a = \frac{\sigma_0 r_p^{\,2}}{2\sqrt{3Ga}} \tag{6}$$

3.3 The Rich-Impellizeri Theory

Rich and Impellizeri [6] modified the elastic-plastic solution of Hoffman and Sachs [4] and included the elastic deformation of the mandrel. They used the same assumptions and the same solutions for estimating stresses as Hoffman and Sachs [4]. Elastic unloading was used to compute the residual stresses, but a compressive yield zone was computed to avoid the violation of the yield criterion near the edge of the hole. The relation between r_p and u_a was developed by matching the radial displacement of the mandrel and the plate. The final form of the expression derived by them for the elastic-plastic boundary, r_p is

$$\frac{u_a}{a} = \frac{\sigma_0}{\sqrt{3}E_b}\left[0.52\left(2\ln\frac{r_p}{a} + 1 - \frac{r_p^2}{b^2}\right) + 1.5\frac{r_p^2}{a^2}\frac{E_b}{E_p}\right] \tag{7}$$

where,

E_b and E_p are the modulus of elasticity of mandrel and plate respectively,
b is the distance from the center of the hole to the edge of the plate,
a is the radius of the hole, and
u_a is the radial expansion.

4.0 FINITE ELEMENT MODEL

4.1 Material properties

Power law relationship is used to generate stress-strain data points for aluminium alloy 2024-T351 material with isotropic hardening behaviour,

$$\varepsilon = \frac{\sigma}{E} \qquad \text{for} \quad \sigma \le \sigma_y$$

and

$$\varepsilon = \frac{1}{E}\left(\frac{\sigma^{n+1}}{\sigma_y^{\,n}}\right) \quad \text{for} \quad \sigma \ge \sigma_y \tag{8}$$

The Finite Element code LUSAS version 13.1[7] has been used to simulate the cold working process under plane stress. The mechanical properties of aluminium alloy 2024-T351 in the longitudinal rolling direction are given in Table 1. The other details are given in a companion paper [8].

4.2 Model geometry, boundary conditions and loading details

The geometrical details of the specimen used to simulate cold-expansion of plate hole are given in Figure 5. The symmetric nature of the model permits construction of a quarter model for the analysis (Fig.6) of cold work in a plate specimen with hole. The model is built using conventional 2D plane stress solid continuum element with enhanced strains (QPM4M), which is a rectangular

element with 4-nodes from family of 2D isoparametric elements with fine integration scheme of 2×2 LUSAS [10]. The mesh is generated automatically using 1725 QPM4M elements in the model (Fig.6). Around the hole region the mesh is refined to increase the density of the elements to obtain convergence of stresses around the hole region for better results. The nodes along the y-axis and x-axis are restrained to move in the *X* and *Y* directions respectively, in view of symmetry of the specimen. The load is applied to the hole edge of the specimen in terms of radial expansion, u_a. A radial expansion of 0.1068 mm is applied at the hole edge giving a cold work of approximately 3.56% as evaluated by Equation (1).

5.0 EXPERIMENTAL RESULTS AND DISCUSSION

The cold working experiment has been carried out as discussed in section 2.5. The voltage signal from sixteen strain gauges (Figure 2) corresponding to three cases i) maximum mandrel insertion condition, ii) relaxation with maximum mandrel insertion condition, after a relaxation period of approximately 2 minutes and iii) mandrel removed condition, as represented by points 3, 4 and 5 in Figure 4 have been recorded and the respective voltage signals have been converted to strain values ε_3, ε_4, and ε_5 using their respective calibration constants given in Table 3. The converted radial strain data at the point 3, 4 and 5 is given in Table 3. The radial strains measured through the sixteen strain gauges mounted in the radial direction around the hole region (Figure 2) have been plotted against radial distance r from the edge of the hole in Figure 7.

It has been observed that the strain values at each measuring locations reduced considerably with respect to the full mandrel insertion after the mandrel is pushed through the specimen completely. It has also been observed that there is no perceptible change in voltage signal beyond the point 5 (Figure 4) for subsequent additional 20 minutes. Hence it is presumed that the voltage signal at point 5 (Figure 4) represent the true voltage signal and there is no further relaxation of strain values when the mandrel is removed from the specimen after the cold work operation is complete. This condition is represented by an almost flat curve region beyond the point 5 in the recorded plot (Fig.4). The difference in strain values from point 3 to point 4 represents strain relaxation of the material around the hole region with mandrel fully inserted condition, while the difference in strain values from the point 3 to point 5 represents the strain reduction when the mandrel is removed with respect to the full mandrel insertion and they are given in percent in Table 3.

As a result of cold working, the region around the hole is plastically deformed. The spread of plastic zone is represented by the elastic-plastic boundary radius, r_p from the center of the hole [4]. At the edge of the hole, the strain is maximum when the mandrel is in the fully inserted condition and it reduces to yield strain of the material at the elastic-plastic interface i.e. elastic-plastic boundary radius, r_p.

Beyond this elastic-plastic boundary radius till the outer edge of the specimen, the material will have elastic stresses and the magnitude of elastic stresses will reduce with the increase in radial distance from the elastic-plastic boundary. The distances from the hole edge corresponding to three cases i) maximum mandrel insertion condition, ii) relaxation with maximum mandrel insertion condition, after a relaxation period of approximately 2 minutes and iii) mandrel removed condition, as represented by points 3, 4 and 5 in Figure 4, for given yield strain of 0.005866 are 4.375 mm, 4.0625 mm, and 3.2031 mm respectively. The elastic-plastic boundary from the center of the hole for maximum mandrel insertion condition is obtained by adding the radius of the hole to the distance from the edge of the hole and is 7.3775 mm. The value of elastic-plastic boundary calculated using closed form solutions based on the existing theories given by Chang [1], Nadai [3], and Rich and Impellizeri [6] for the maximum mandrel insertion condition are 6.3769 mm, 8.54 mm, and 7.71 mm respectively. The value of elastic-plastic boundary obtained experimentally for maximum mandrel insertion condition is 7.3775 mm and it compares well with the above-mentioned theories. A plane stress elastic-plastic finite element analysis is carried out with a radial expansion of 0.1068 corresponding to a cold work of 3.56%. It has been observed from the tangential residual stress distribution under loading condition i.e. under maximum mandrel insertion condition that the elastic-plastic boundary from the edge of the hole is at 5.9195 mm, which is quite close to the experimental results of this analysis. This comparison is done to show the authenticity of the experimental work carried out. The finite element results for the tangential residual stress distribution data are not shown here as the analysis for radial strain is stressed here.

The radial strain distribution data, obtained using elastic-plastic finite element analysis, is plotted against the radial distance from the edge of the hole in Figure 8. This radial strain is the residual radial strain, which represents the complete mandrel removed condition. The radial distance corresponding to yield strain of 0.005866 is 2.917 mm from the edge of the hole (Figure 9). The radial strain distribution data obtained experimentally and through finite element analysis are shown together in Figure 9. The experimental residual radial strain distribution results (Figure 9) compare very well with the FEM results for full mandrel removed condition represented by point 5 in Figure 4. The following power law relation gives the residual radial strain corresponding to point 5 (Figure 4),

$$\varepsilon_r = 0.00467 r^{-1.7829} \tag{9}$$

The radial strain relaxation and radial strain reduction values are calculated with the following equations and are plotted against the radial distance from the edge of the hole in Figure 10.

$$\varepsilon_{relx} = \frac{\varepsilon_4 - \varepsilon_3}{\varepsilon_3} \times 100\ \% \tag{10}$$

$$\varepsilon_{red} = \frac{\varepsilon_5 - \varepsilon_3}{\varepsilon_3} \times 100\ \% \qquad (11)$$

The radial strain relaxation, ε_{relx} is approximately 10 to 15 %, and the radial strain reduction, ε_{red} is approximately 20 to 30 % (Table 3) for radial distances from the edge of the hole till the elastic-plastic boundary (Fig.10). On the other hand, the radial strain reduction is in the range of 50 to 78% for the elastic region beyond the elastic-plastic boundary. The radial strain relaxation data can be used to assess the residual strain in the specimen for a case of maximum mandrel insertion condition, which is of practical importance for developing the fatigue crack propagation models.

6.0 CONCLUSIONS

The following conclusions are drawn based on the experimental results of the present investigation,

i) The strain relaxation data has been obtained for maximum mandrel inserted condition, with respect to elapsed period of relaxation of 2 minutes condition, and the strain reduction data for fully mandrel-removed condition.
ii) The value of elastic-plastic boundary experimentally determined matches well with the existing theories of Nadai, Chang, and Rich and Impellizeri.
iii) The experimental residual radial strain distribution results compare very well with the FEM results particularly for a case of full mandrel removed condition.
iv) The recommendation is made to use the strain relaxation data for a case where the mandrel need not be removed after cold working for assessing the residual strain distribution in the specimen.

ACKNOWLEDGEMENT

The authors gratefully acknowledge the financial support of Ministry of Science, technology & Environment, Malaysia (IRPA Project No.03-02-04-0089), for the first provision of a research grant for this work.

NOMENCLATURE

a	Initial radius of the hole
E	Young's modulus
ν	Poisson's ratio
r_p	Elastic-plastic boundary
u_a	Radial expansion
u_{aE}	Elastic radial expansion
σ_r	Radial stress
σ_θ	Tangential stress
σ_o	Yield stress
ε_r	Radial strain
ε_θ	Tangential strain
G	Shear modulus
R	Resistance of the strain gauge
R_{cal}	Calibration resistance
GF	Gauge factor
ε_{relx}	Strain relaxation
ε_{red}	Strain reduction

REFERENCES

1. Chang, J.B., 1977, "*Prediction of fatigue crack growth at cold worked fastener holes*", Journal of Aircraft, Vol. 14. No.9, pp 903-908.
2. Poolsuk, S. and Sharpe, Jr, W.N., 1978, "*Measurement of the elastic-plastic boundary around cold worked fastener hole*", Journal of Applied Mechanics Vol. 45, pp 515-520.
3. Dally, James W. and Riley, William F., 1965, "*Experimental stress analysis*", McGraw Hill Book Company, N.Y.
4. Hoffman, O. and Sachs, G., 1953, "*Introduction to the theory of plasticity for engineers*", McGraw Hill New York, pp 80-95.
5. Nadai, A., 1943, "*Theory of the expanding of boiler and condenser tube joints through rolling*", Transaction of the ASME, Vol. 65, pp 865-880.
6. Rich, D.L. and Impellizeri, L.F., 1977, "*Fatigue analysis of cold worked and interference fit fastener holes*", Cyclic stress strain and plastic deformation aspects of fatigue crack growth, STP 637, American Society of Testing Materials, Philadelphia, pp 154-175.
7. LUSAS (London University Stress Analysis System), 2001, FEA Ltd Forge House, 66 High Street, Kingston upon Thames, Surrey, KTI 1Hn, United Kingdom.
8. Arora, P. R., Jeffrey, Tan M.L., Christian, B., and Waqar, A., 2^{nd} – 3^{rd} October 2001, "*Finite element analysis of residual stresses for cold working in a 2024-T351 aluminium alloy plate*", Proceedings UPM Engineering Research Seminar, Faculty of Engineering, University Putra Malaysia, pp 118-133.

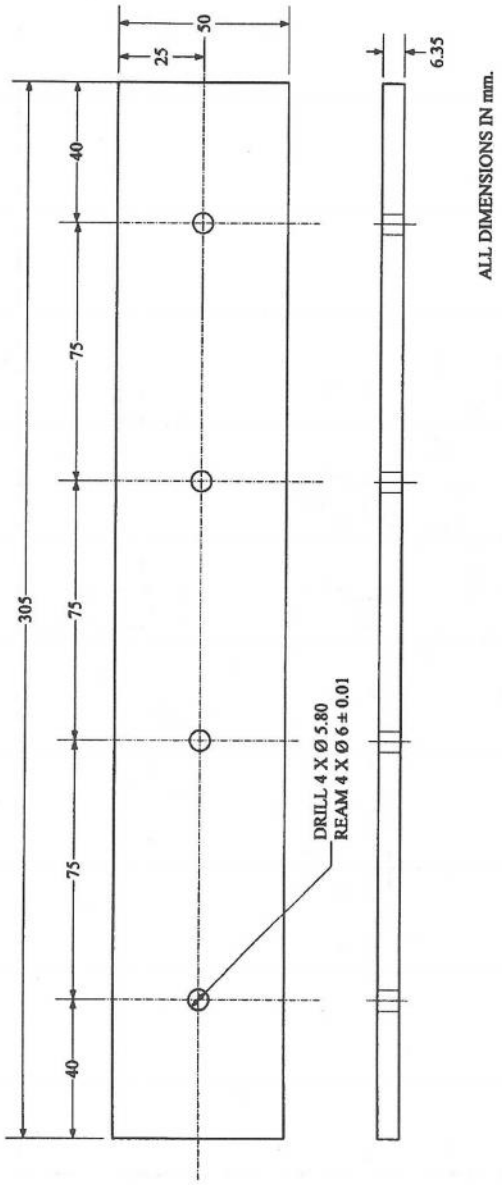

Figure 1 Specimen Geometry

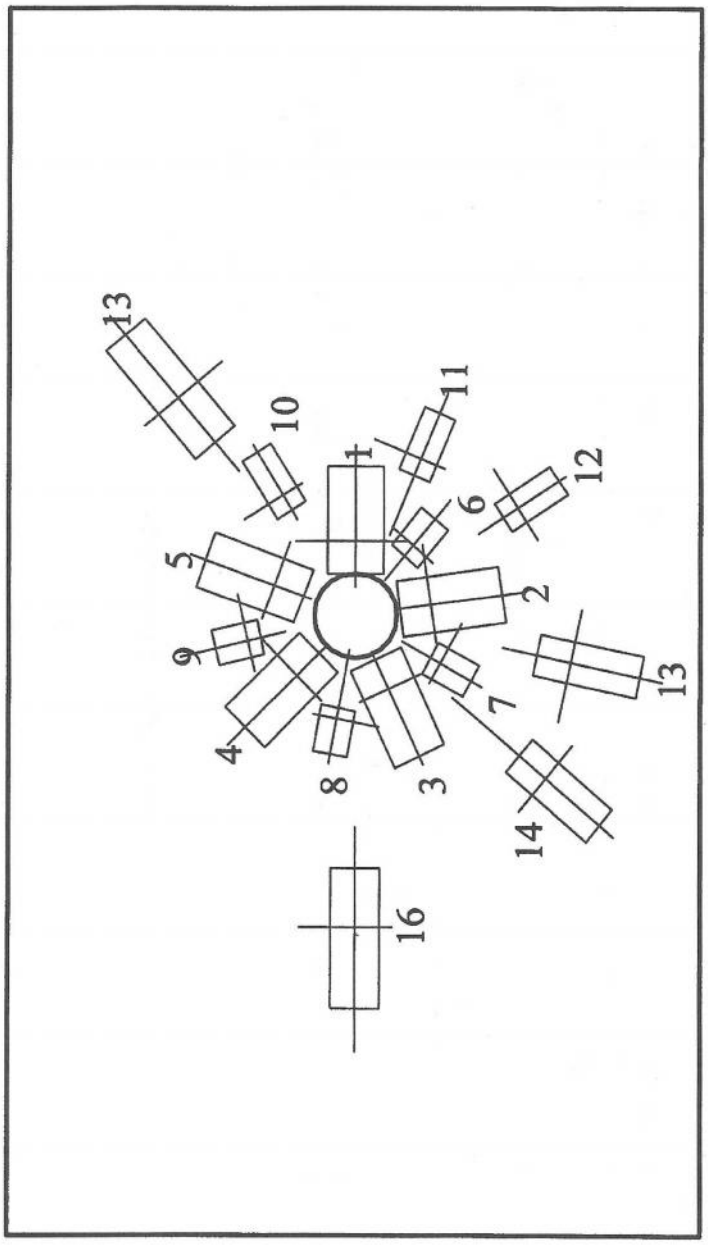

Figure 2 Location of strain gauges around the hole

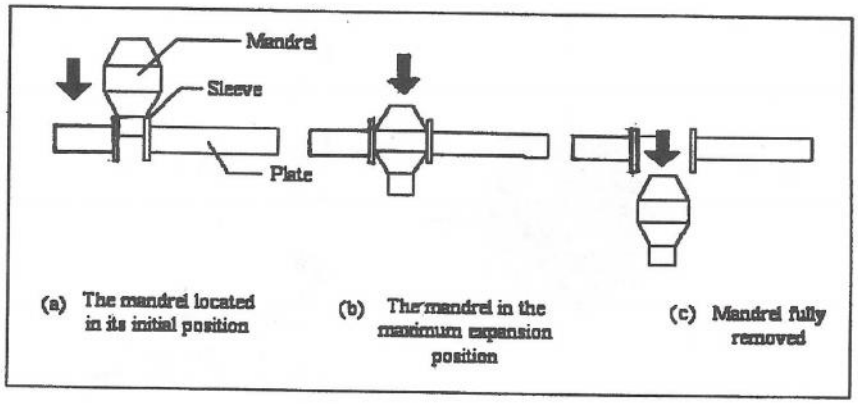

Figure 3 Stages of the cold working as the mandrel is pushed through the hole

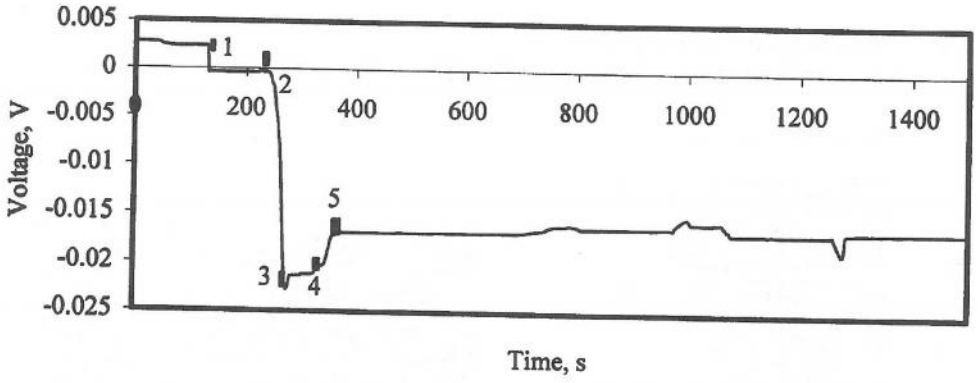

Figure 4 Variation in voltage singal versus time (strain gauge no. 1)

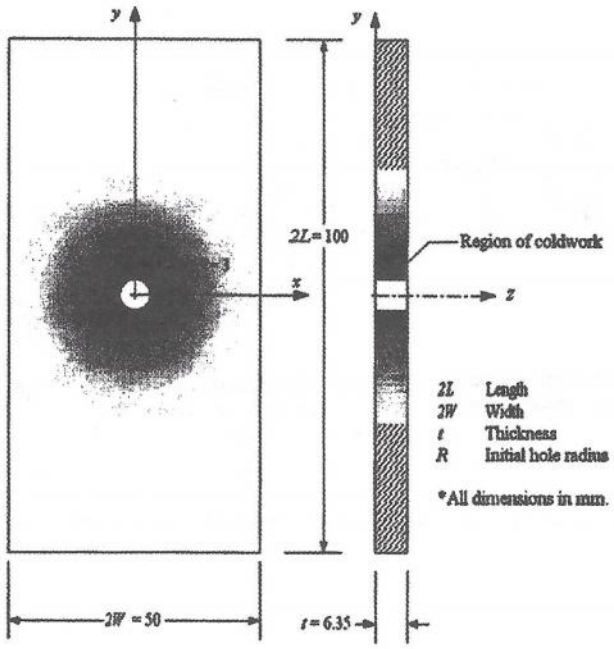

Figure 5 Model specimen details

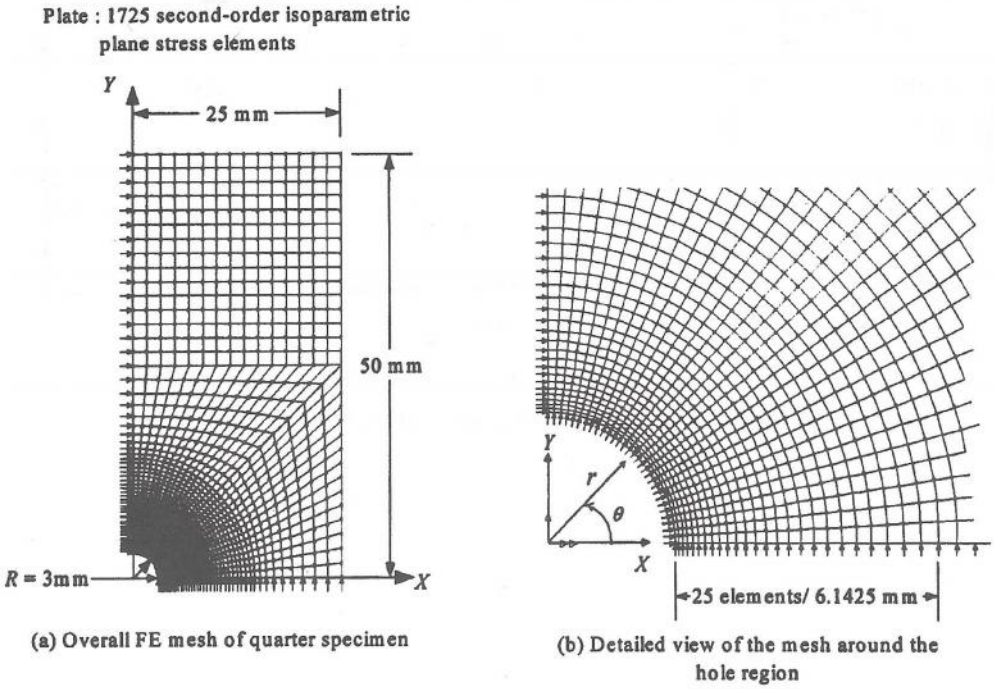

Figure 6 Two-dimensional FE model with uniform radial expansion loading along the hole perimeter

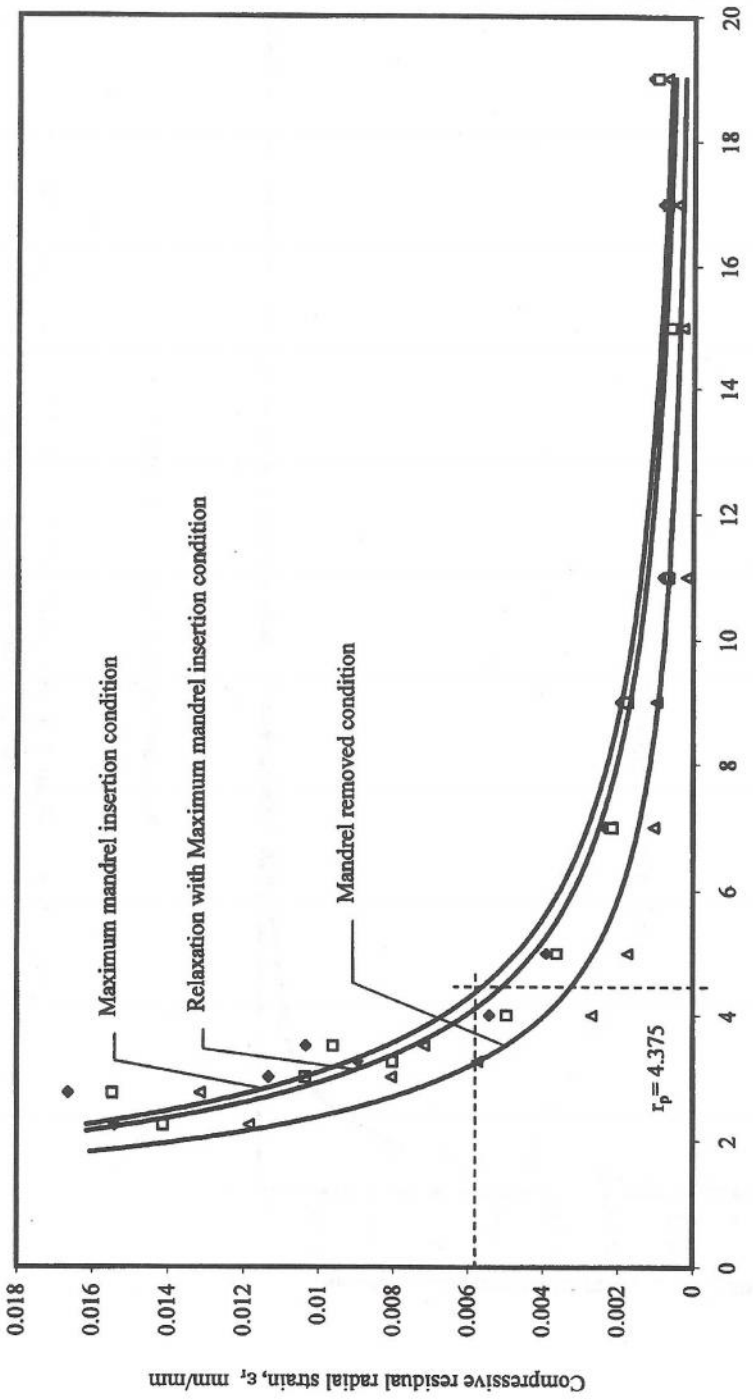

Figure 7 Radial strain versus radial distance from the hole edge

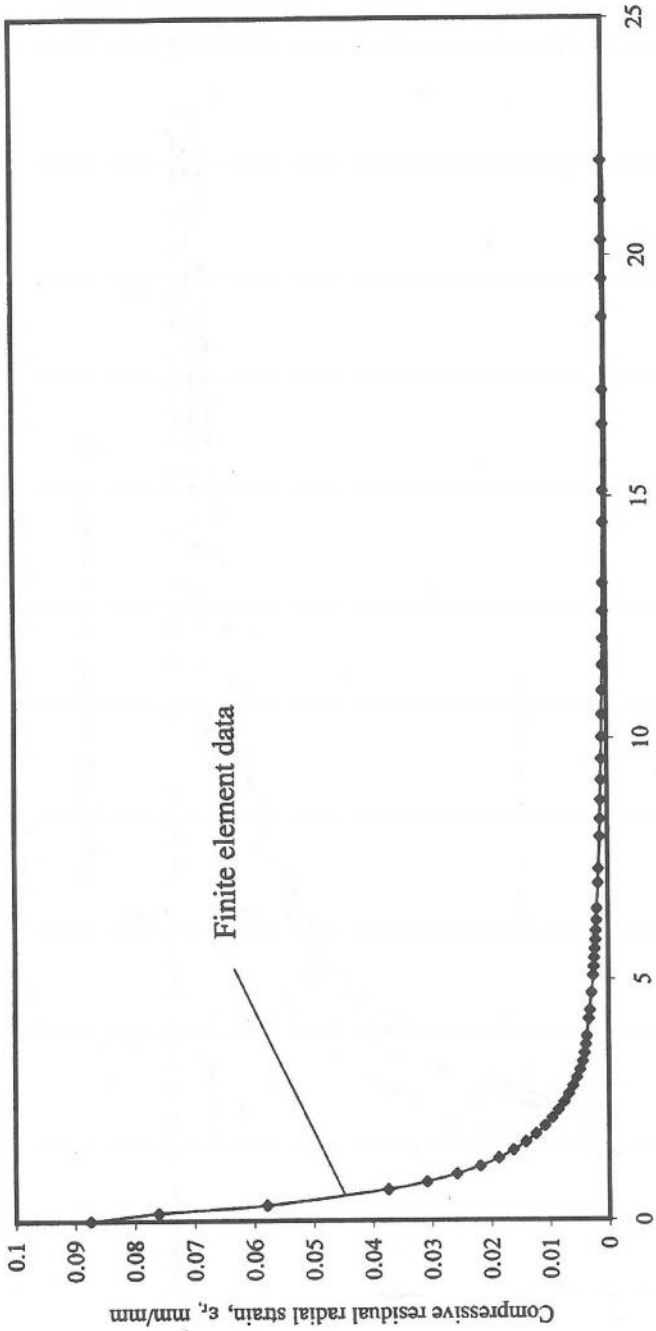

Figure 8 Radial strain versus radial distance from the edge of the hole for full mandrel removed condition

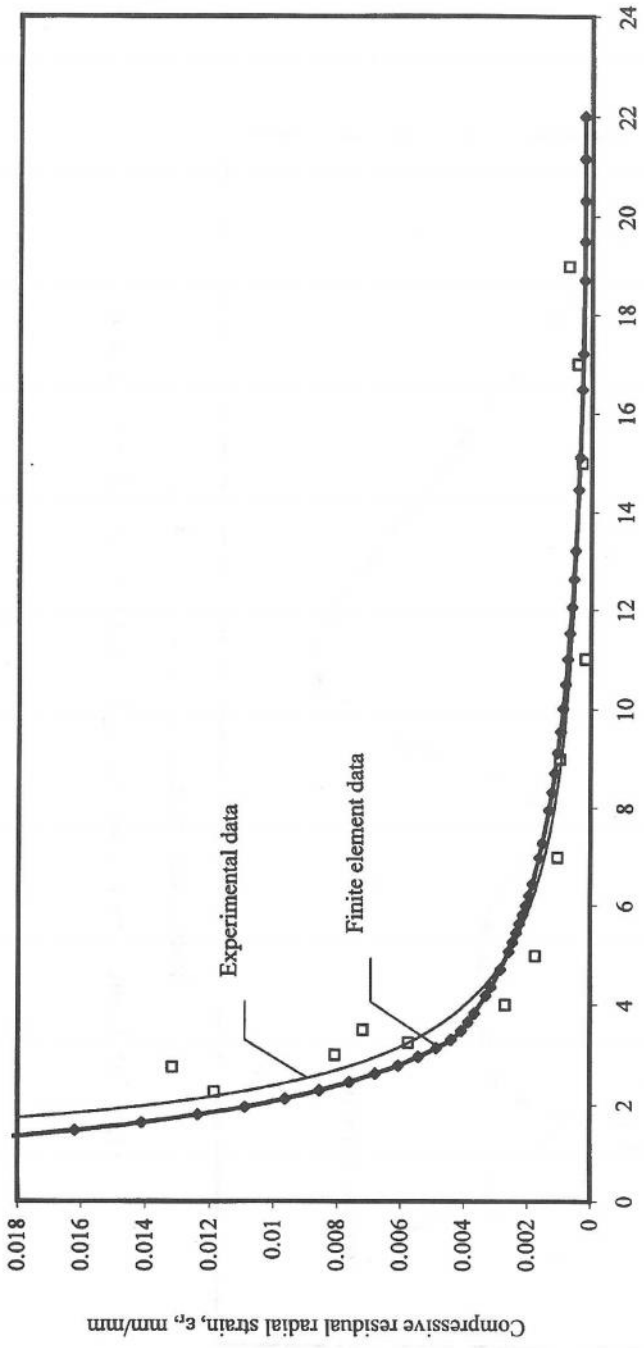

Figure 9 Radial strains versus radial distance from the edge of the hole for full mandrel removed condition

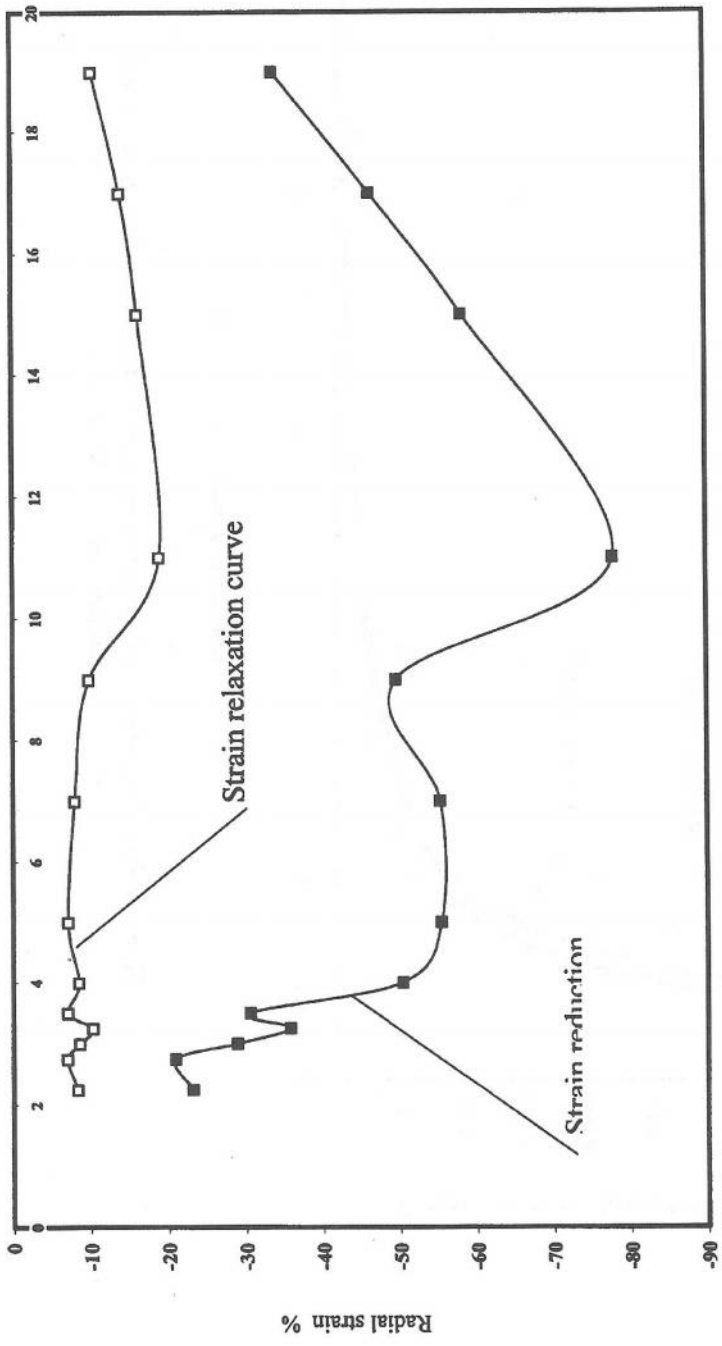

Figure 10 Radial strain versus radial distance from the edge of the hole

Table 1 Mechanical properties of aluminium alloy 2024 T-351

Properties	Magnitude
Ultimate tensile strength (MPa)	620
Yield Strength (MPa)	420
Modulus of Elasticity (MPa)	71593
Poisson's Ratio	0.28

Table 2 Strain gauge mounting and calibration details

Gauge No	Gauge Length (mm)	Gauge Width (mm)	Radial Distance from Edge of Hole (mm)	Calibration Constant
1	7.5	4.0	2.25	0.7015
2	7.5	4.0	2.5	*
3	7.5	4.0	2.75	0.7623
4	7.5	4.0	3.0	0.7660
5	7.5	4.0	3.25	0.7603
6	3.35	2.5	3.5	0.7652
7	3.35	2.5	4.0	0.7626
8	3.35	2.5	4.5	*
9	3.35	2.5	5.0	0.7029
10	4.8	2.4	7.0	0.7011
11	4.8	2.4	9.0	0.7656
12	4.8	2.4	11.0	0.7527
13	7.6	3.0	13.0	0.7485
14	7.6	3.0	15.0	0.7578
15	10.0	3.6	17.0	0.7688
16	10.0	3.6	19.0	0.7538

Common gauge factor, GF = 2.12, * damaged gauges

Table 3 Radial strain data

Gauge No	Distance from Hole Edge (mm)	ε_3	ε_4	ε_5	Radial Strain Relaxation (%)	Radial Strain Reduction (%)
					$\%(\varepsilon_4-\varepsilon_3)/\varepsilon_3$	$\%(\varepsilon_5-\varepsilon_3)/\varepsilon_3$
1	2.25	0.015416	0.014127	0.01185	-8.362	-23.137
3	2.75	0.016639	0.015469	0.013157	-7.029	-20.926
4	3	0.011332	0.010354	0.008055	-8.629	-28.916
5	3.25	0.008944	0.00802	0.005745	-10.327	-35.767
6	3.5	0.010336	0.009606	0.007175	-7.066	-30.582
7	4	0.005429	0.004967	0.002691	-8.521	-50.427
9	5	0.003906	0.003627	0.00174	-7.130	-55.457
10	7	0.00233	0.002144	0.001041	-7.981	-55.329
11	9	0.001929	0.001739	0.000971	-9.865	-49.654
12	11	0.000808	0.000655	0.000179	-18.973	-77.909
14	15	0.00071	0.000594	0.000296	-16.263	-58.331
15	17	0.000807	0.000693	0.000432	-14.074	-46.402
16	19	0.00109	0.000975	0.000721	-10.533	-33.830